

Single-molecule DNA sequencing using two-dimensional $\text{Ti}_2\text{C}(\text{OH})_2$ MXene nanopores: A first-principles investigation

Jariyanee Prasongkit¹ (✉), Sirichok Jungthawan^{2,3,4}, Rodrigo G. Amorim⁵, and Ralph H. Scheicher⁶ (✉)

¹ Division of Physics, Faculty of Science, Nakhon Phanom University, Nakhon Phanom 48000, Thailand

² School of Physics, Institute of Science, Suranaree University of Technology, 111 University Ave, Nakhon Ratchasima 30000, Thailand

³ Center of Excellence in Advanced Functional Materials, Suranaree University of Technology, Nakhon Ratchasima 30000, Thailand

⁴ Thailand Center of Excellence in Physics, Ministry of Higher Education, Science, Research and Innovation, 328 Si Ayutthaya Road, Bangkok 10400, Thailand

⁵ Departamento de Física, ICEx, Universidade Federal Fluminense-UFF, Volta Redonda/RJ 27213-145, Brazil

⁶ Division of Materials Theory, Department of Physics and Astronomy, Uppsala University, Uppsala SE-751 20, Sweden

© The Author(s) 2022

Received: 21 December 2021 / Revised: 7 May 2022 / Accepted: 1 June 2022

ABSTRACT

Nanopore-based devices have provided exciting opportunities to develop affordable label-free DNA sequencing platforms. Over a decade ago, graphene has been proposed as a two-dimensional (2D) nanopore membrane in order to achieve single-base resolution. However, it was experimentally revealed that clogging of the graphene nanopore can occur due to the hydrophobic nature of graphene, thus hindering the translocation of DNA. To overcome this problem, the exploration of alternative 2D materials has gained considerable interest over the last decade. Here we show that a Ti_2C -based MXene nanopore functionalized by hydroxyl groups ($-\text{OH}$) exhibits transverse conductance properties that allow for the distinction between all four naturally occurring DNA bases. We have used a combination of density functional theory and non-equilibrium Green's function method to sample over multiple orientations of the nucleotides in the nanopore, as generated from molecular dynamics simulations. The conductance variation resulting from sweeping an applied gate voltage demonstrates that the Ti_2C -based MXene nanopore possesses high potential to rapidly and reliably sequence DNA. Our findings open the door to further theoretical and experimental explorations of MXene nanopores as a promising 2D material for nanopore-based DNA sensing.

KEYWORDS

nanopore, DNA sequencing, MXenes, first-principles, quantum transport

1 Introduction

Nanopore-based DNA sequencing allows for ultra-fast and reliable sequencing of genomes including the human genome [1–4]. A major advantage of nanopores is that they can facilitate label-free, high-throughput, and ultra-long reads, and require few reagents [5]. Nanopore sequencing devices can be broadly classified into two categories [6]: biological [7–9] and solid-state. Under an applied bias voltage, an ionic current signal is generated. When a DNA molecule passes through the nanopore, it causes a corresponding current blockade, thus revealing different types of nucleotides at the single-molecule level [10, 11]. On the other hand, an alternative approach is based on measuring the transverse electronic current of single-stranded DNA passing through the nanopores to analyze the nucleotide sequence [12–15]. Using the latter approach, solid-state devices have a benefit, since part of the membrane can be fabricated from conductive materials. Furthermore, solid-state nanopores also offer many advantages over their biological counterparts, such as mechanical robustness, chemical stability, easy modification, and large-scale integration [16, 17]. In combination with field-effect transistors (FETs), they can be integrated on a chip with other electronic components, providing the potential for powerful,

portable, and real-time devices. However, there are some drawbacks of the solid-state nanopore fabrication for DNA sequencing, such as being time-consuming and lacking the resolution to create pores with controllable size to detect individual nucleotides [18, 19].

With advances in nanotechnology, in 2010, several research groups have experimentally demonstrated that graphene nanopores can be used to study the DNA translocation process [20–22]. Graphene membranes, one atomic layer of carbon atoms with extraordinary electrical and mechanical properties, can solve the problem of alignment [23]. Nanopores can be fabricated by controlled electron-beam exposure via transmission electron microscopy (TEM) in which the diameter can be precisely controlled at sub-nanometer resolution [24]. While graphene may hold the potential to achieve single-nucleotide resolution, major disadvantages remain, such as large noise and poor mechanical stability [25–27]. For the sake of completeness, it is worth to point out here that there also exist alternative DNA sequencing techniques utilizing graphene, such as nano-channels in combination with two-dimensional (2D) molecular electronics spectroscopy [28].

In recent years, other 2D materials beyond graphene, such as

Address correspondence to Jariyanee Prasongkit, jariyanee.prasongkit@npu.ac.th; Ralph H. Scheicher, ralph.scheicher@physics.uu.se

hexagonal boron nitride (h-BN) [29, 30], molybdenum disulfide (MoS_2) [31–33], and tungsten disulfide (WS_2) [34], have opened up new possibilities for improving the efficiency of solid-state nanopore sensors and have been exploited for DNA sensing with nanopores. More recently, MXenes, a new family of 2D transition metal carbides [35], have become another choice for nanopore-based DNA sequencing due to their relatively easy fabrication process and versatile chemistry. The general formula of MXenes is $M_{n+1}X_nT_x$ ($n = 1, 2, 3$), where M is a transition metal, X is C and/or N, and T indicates a surface termination (F, O, or OH groups) on the MXene surface [35, 36]. MXenes can provide excellent electrical properties and good stability with tunable surface functionality [37], and therefore serve as the motivation of our work to explore the performance of MXenes for DNA detection devices. Mojtabavi et al. [38] have experimentally demonstrated the feasibility of MXenes (Ti_2CT_x and $\text{Ti}_3\text{C}_2\text{T}_x$) as nanopore membranes for sequencing DNA. It has been indicated that MXene membranes provide a low ion current leakage, and the noise level is comparable to those of other 2D membranes. Additionally, at least one theoretical study [39] assessed the potential of Ti_3C_2 MXenes for DNA detection using molecular dynamics (MD) simulation. Based on the measurements of ionic currents through Ti_3C_2 nanopore, they successfully detect different types of DNA bases. So far, however, the feasibility of MXenes as nanopore membranes for DNA sequencing utilizing the transverse electronic transport channel has not yet been assessed. In this work, we use state-of-the-art first-principles methods to evaluate whether the MXenes $\text{Ti}_2\text{C(OH)}_2$ can act as a reliable DNA sequencing device.

To this end, by using a combination of density functional theory (DFT) and non-equilibrium Green's functions (NEGF) method [40, 41], we have assessed the potential of MXene nanopores proposed for DNA sequencing. We investigated the electrical transport properties, allowing for orientational fluctuations of individual nucleotides as they pass through the $\text{Ti}_2\text{C(OH)}_2$ MXene nanopore. The trajectory of molecular structures for the transport calculations was obtained using quantum MD simulations at room temperature. We indicate that the interaction between the nucleobase and the pore edge enables different electrical properties and reduces translocation speed. To make this approach practical as a DNA-FET, we have further taken into account the modulation of an applied gate voltage to resolve the signal overlap between different nucleobases. By analyzing the transmission pathway, it is revealed that the difference in conductance values due to the gate voltage tuning significantly depends on the individual electronic signatures of each nucleobase. All optimizations were performed using DFT [42, 43] in the generalized gradient approximation of Perdew, Burke, and Ernzerhof (GGA-PBE) [44], as implemented in the QuantumATK software [45].

2 Methodology

The nucleotides and the MXene were first optimized separately. Four naturally occurring nucleotides, deoxyguanosine monophosphate (dGMP), deoxyadenosine monophosphate (dAMP), deoxycytidine monophosphate (dCMP), and deoxythymidine (dTTP), for simplicity in the following, were abbreviated only as G, A, C, and T, respectively. For nanopore construction, the unit cell of $\text{Ti}_2\text{C(OH)}_2$ was relaxed and repeated in both the x and z directions for device simulation. A single-zeta basis set with polarization orbitals (SZP) along with norm-conserving pseudopotentials [46] was employed for all atoms, which had already been proven to be a valid approach for the theoretical investigation of the MXene nanodevice system [47].

For supercell calculations, the mesh cutoff was set to 150 Ry for the real-space grid, and the Monkhorst-Pack scheme [48] was used with a mesh of $5 \times 1 \times 5$ k -points for the Brillouin zone integration. Structural relaxations were carried out until residual forces on each ion were less than 0.01 eV/Å. Then the nucleotides were placed inside the nanopore and quantum MD simulation was performed to investigate the motion of nucleotides. The same energy cut-offs were used in the DFT-MD calculations and only the Gamma point was considered for Brillouin zone sampling. The nanopore was kept fixed while the nucleotide was allowed to freely move around the nanopore. The simulations were performed in the microcanonical (NVE) ensemble for equilibration for 5 ps, followed by the canonical (NVT) ensemble using a Nosé-Hoover thermostat at 300 K with a time step of 1 fs. After an equilibration time of 10 ps, snapshots of the configuration were taken at every 0.5 ps to calculate the corresponding transport properties.

To investigate the electronic coupling between the nucleotide and the nanopore, the binding energy (E_b) was calculated as

$$E_b = (E_{\text{pore}} + E_{\text{nucleotide}}) - E_{\text{total}} + E_{\text{BSSE}} \quad (1)$$

where E_{total} is the total energy of the system (pore + nucleotide), and E_{pore} and $E_{\text{nucleotide}}$ are the energies of $\text{Ti}_2\text{C(OH)}_2$ nanopore and nucleotide alone, respectively. The basis set superposition error (BSSE) has been accounted for by using the counterpoise (CP) correction technique [49].

The nanopore-based device used to calculate the electronic transport properties is shown in Fig. 1(a). The simulation cell had a width of 3.18 nm (x -direction), and a length of 3.68 nm (z -direction). The total number of simulated atoms, including the nucleotide within the nanopore, was approximately 1,300 atoms. The cell was created with sufficiently large vacuum regions to avoid any nonphysical interactions. The diameter of the pore was around 1.6 nm, allowing only one nucleotide at a time to be accommodated inside the nanopore in every possible orientation. The setup was divided into three parts: a central region (C) enclosed by the semi-infinite left (L) and right (R) electrodes. The $\text{Ti}_2\text{C(OH)}_2$ was periodic in the x -direction, while in the z -direction it was attached to semi-infinite periodic structures. Using the NEGF technique based on DFT as implemented in the QuantumATK package [45], the transmission probability of electrons with energy E from the left electrode to reach the right

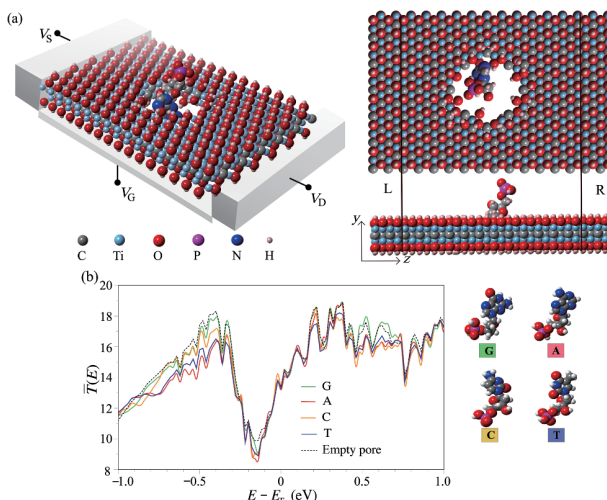


Figure 1 (a) Illustration of the $\text{Ti}_2\text{C(OH)}_2$ MXene nanopore-based device for measuring the conductance while the four nucleotides (G, A, C, and T) are translocated through the nanopore. (b) The average transmission spectra of the four nucleotides for selected snapshots from MD simulation, as compared to the spectrum of the empty nanopore.

electrode—passing through the central region—was given by

$$T(E) = \text{Tr}[\Gamma_R(E) G^R(E) \Gamma_L(E) G^A(E)] \quad (2)$$

where $\Gamma_{L(R)}(E)$ is the coupling matrix of the left (right) electrode, and $G^{R(A)}(E)$ is the retarded (advanced) Green's function [40]. At equilibrium under zero bias, the conductance could be related to the transmission via the Fisher–Lee relation [50]

$$G = G_0 T(E_F) \quad (3)$$

where $G_0 = 2e^2/h$ is the quantum conductance.

The transmission pathway was investigated by splitting the transmission coefficient between each pair of adjacent sites into local bond contributions, T_{ij} . The system was divided into two parts (A and B), allowing us to calculate the pathway across the boundary A and B by summing up to the total transmission coefficient

$$T(E) = \sum_{i \in A, j \in B} T_{ij}(E) \quad (4)$$

where $T_{ij}(E)$ is the local bond contributions for each pair of adjacent sites (i, j) at a specific energy E . The transmission pathway (or local current) consists of the $T(E)$ projection between two sites (M and N). Using the Keldish formalism [41], the current density $i(E)$ could be written between two sites N and M as a sum involving the spectral function and the Hamiltonian element, with the sum running over all localized atomic orbitals n and m of the basis set, which were associated with sites N and M, respectively. For further details, the works of Solomon et al. [51] and of Paulsson and Brandbyge [52] were referred.

3 Results and discussion

We start our analysis by looking at the zero-bias transmission spectra averaged over 20 electronic transport calculations as a function of energy for the four different nucleotides (G, A, C, and T), as compared to the setup in the absence of nucleotides (see Fig. 1(b)). The magnitudes of the transmission at the Fermi level are much higher than what has been reported in other 2D nanopores, including graphene [53–55], silicene [56, 57], and phosphorene [58]. This implies that the $\text{Ti}_2\text{C}(\text{OH})_2$ nanopore has opened many conduction channels owing to the partially occupied d-shells of Ti atoms, which can significantly reduce the current noise and improve the signal-to-noise ratio in nanopore experiments [59]. Although the transmission profile depends on their positions and orientations inside the nanopore, it is quite clear from averages of the transmission over snapshots that the device is still able to preserve its ability to selectively discriminate different nucleotides. The variation in peak height of the transmission could arise from the interaction between the nucleotides and the nanopore as well as from the specific electronic signatures of each nucleotide, as will be further discussed below.

To understand the correlation between the electronic coupling of DNA with the $\text{Ti}_2\text{C}(\text{OH})_2$ nanopore and the charge transport in the device, we estimated the nucleotide conductance at equilibrium under zero bias of the selected snapshots for G, A, C, and T. Note that the snapshots were chosen with the transmission at the Fermi energy close to the average values. In Fig. 2(a), the correlation between transport and coupling of the nucleotide was demonstrated by presenting the nucleotide conductance as a function of binding energy. We found the conductance under zero bias to drop with increasing binding energy. Such a relationship between the conductance and the binding energy reveals that the charge transport in devices is significantly affected by the electronic coupling around the nanopore edge.

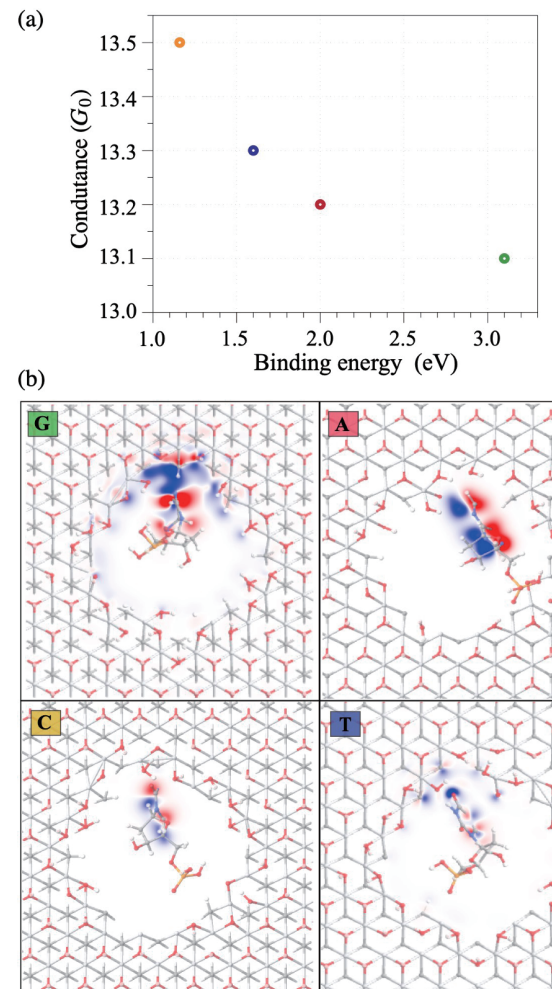


Figure 2 (a) Conductance vs. binding energy and (b) contour map of electron charge density difference of the G, A, C, and T nucleotides inside the nanopore. For the contour map plots, red color represents negative charge density difference while blue corresponds to a positive change in charge density.

To further gain an insight into the interaction of DNA nucleotides with the nanopore, the total charge density redistribution was calculated by using the expression

$$\Delta\rho(r) = \rho_{\text{device+nucleotide}}(r) - (\rho_{\text{device}}(r) + \rho_{\text{nucleotide}}(r)) \quad (5)$$

where $\rho_{\text{device+nucleotide}}(r)$ is the total charge density of the device and nucleotide together, $\rho_{\text{device}}(r)$ is the charge density of the nanodevice alone, and $\rho_{\text{nucleotide}}(r)$ is the charge density of the nucleotide by itself. Our results for $\Delta\rho(r)$ are presented in Fig. 2(b). The charge density difference fluctuates mostly at the pore edges close to the base, leading to conductance alterations of the device. We found G and A to provide higher electron reorganization which brings about the reduction of electron charge transport as compared to the other two nucleotides. In other words, a strong base-nanopore interaction would decrease the conductance value.

Next, we explored how the conductance could be affected via gate voltage control. In experimental studies, the Fermi level can be tuned by adjusting external gate voltages. Thus, the transmission function could be replaced by the conductance at a small bias as a function of gate voltage (V_g)

$$G(V_g) = (2e^2/h)T(\mu) \quad (6)$$

where h is Planck's constant and $\mu = E_F - eV_g$. The conductance measurement can allow a clear distinction of changes in the electrical signal since the conductance of the device changes by the

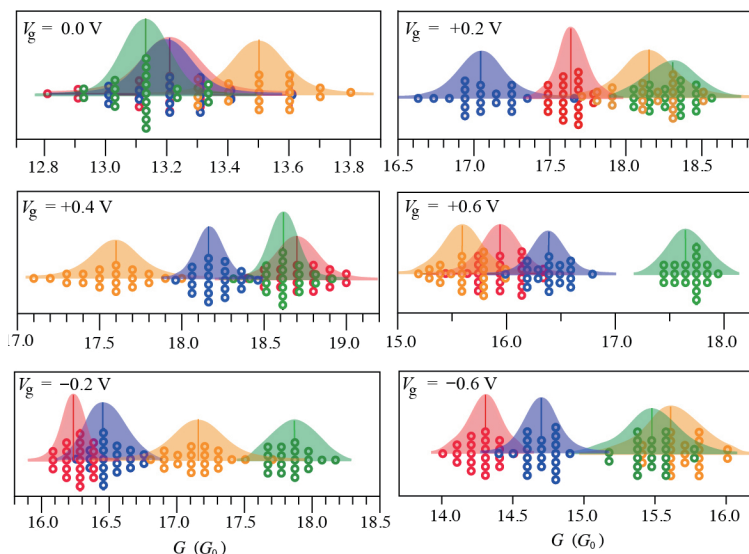


Figure 3 Conductance distribution curves over selected trajectory snapshots of G (green), A (red), C (orange), and T (blue) for a range of gate voltages from -0.6 to 0.6 V.

quantum conductance unit G_0 .

Figure 3 demonstrates the conductance $G(V_g)$ distribution curves from selected trajectory snapshots of each nucleotide for a range of gate voltages from -0.6 to 0.6 V. The spread in conductance values is attributed to a variation in orientation and position of the nucleotides during translocation through the nanopore. At the gate voltage of $V_g = 0.0$ V, one can see each nucleotide has a well-defined maximum and broad tails on both sides of it. The peak position indicates the conductance of preferential configuration and orientation of the nucleotides passing through the nanopore, while the peak width indicates the degree of their variation. It was seen that the orientational fluctuations of nucleotides cause overlaps of the conductance distributions so that it is difficult to differentiate nucleotides from each other. As depicted in Fig. 3, the signal overlap between different nucleotides can be resolved by sweeping the V_g from -0.6 to 0.6 V. For a whole sweep of chemical potential, the shift in conductance would be unique for each nucleotide.

3.1 Residence time analysis

Another important aspect is the residence time of the nucleotides inside the nanopore. In practical applications, the translocation time can be determined by both DNA lengths and their orientations [60, 61] which contain information about chemical interactions correlated to the binding energies. The residence time (τ) for each DNA base type is proportional to $\sim \exp(E_b/k_B T)$, where E_b is the binding energy, k_B is the Boltzmann constant, and T is the temperature. In Fig. 2(a), the binding energies of each nucleotide inside the nanopore for selected snapshots were found to be 3.07, 2.04, 1.12, and 1.61 eV for G, A, C, and T, respectively. The two purine bases (G and A) have larger polarizabilities than the two pyrimidine bases (C and T); therefore, the latter interacts with the pore weaker than the former. Between G and A, the former exhibits larger binding energy ($E_b > 3$ eV) due to its possession of a double-bonded oxygen atom.

Based on their size, the purine bases are larger, thus requiring a longer time to translocate across the pore. On the other hand, the pyrimidine bases have lower polarizability and smaller size, giving rise to decreased binding energies ($E_b < 2$ eV) and shorter residence times. Compared to other 2D materials [62] such as graphene [54, 55], phosphorene [58], and silicene [57, 63], the $\text{Ti}_2\text{C}(\text{OH})_2$ nanopore exhibits higher binding energies with the DNA bases, which would result in slower translocation speed and

therefore higher read-out accuracy on the DNA sequences. When compared to DNA base interaction with MoS_2 nanopore [64], the binding energies of MoS_2 with each base are in the range from 1.60 to 4.31 eV in the case of Mo-terminated edge. The case of $\text{Ti}_2\text{C}(\text{OH})_2$ exhibits slightly lower binding energies, however, in our study it should be noted that we first filled the $\text{Ti}_2\text{C}(\text{OH})_2$ nanopore with water molecules and relaxed the setup. The pore edges are terminated by hydroxyl groups due to the dissociation of water molecules, which agrees well with the previous studies of water adsorption on the MXene surface [65]. Consequently, the binding energies of our devices originate from the interaction between lone pair electrons on atoms (e.g., O or N) of the nucleobases and the $\text{Ti}_2\text{C}(\text{OH})_2$ nanopore whose edge atoms are terminated with a hydroxyl group. Additionally, our results are in line with a previous study [39] that characterizes the residence time of the DNA base in the Ti_3C_2 MXene membrane. It was revealed that the pyrimidine bases have smaller sizes and translocate faster than the purine bases. By using the MD simulation approach, we observed that the pyrimidine nucleotides in the $\text{Ti}_2\text{C}(\text{OH})_2$ nanopore move freely within the nanopore, whereas the purine nucleotides prefer to stick to the pore edge. Nevertheless, overall our resulting configurations indicate that all nucleotides tend to be attracted by the pore edge, rather than residing at the center. A more detailed discussion of MD trajectories of each nucleotide inside the $\text{Ti}_2\text{C}(\text{OH})_2$ nanopore can be found in the Electronic Supplementary Material (ESM).

3.2 Conductance analysis

To analyze the underlying mechanism leading to the difference in the conductance values presented above, we extracted one snapshot of each nucleotide at $V_g = +0.2$ V as an example. The conductance values have been ordered in the following way: $G_G \simeq G_C > G_A > G_T$. The transmission pathway was investigated to show how the electrical current flows through the device, as presented in the top panel of Fig. 4. The arrows point to the direction of the current flowing from the left to the right electrode, and the blue and red colors indicate the magnitude of the local current flowing through the path. In the case of purine nucleotides which contain a pyrimidine ring fused with an imidazole ring, the current flows through both rings on the G base, whereas for the A base it is observed only on the pyrimidine ring. As a result, A has lower conductance than G. For the pyrimidine nucleotides, the current can easily flow through the cytosine base, but it is entirely

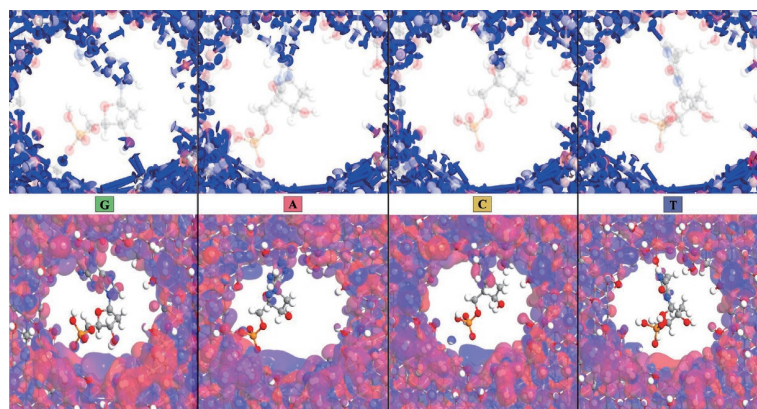


Figure 4 A comparison of the four nucleotides at $V_g = +0.2$ V. The local currents of the specific snapshots for G, A, C, and T nucleotides are plotted in the top panel, and the scattering eigenstates are shown in the bottom panel.

reflected at the atoms of thymine close to the pore edge. As a result, T exhibits lower conductance than C. Interestingly, for all nucleotides, the local current traveling from the nanopore to the base cannot penetrate to the sugar-phosphate group, and the high current density localized over the nanopore edge close to the sugar-phosphate group. For more clarity, in the bottom panel of Fig. 4, we also show the eigenchannel wavefunction corresponding to a scattering state coming from the left electrode and traveling towards the right at $V_g = +0.2$ V. All wavefunctions are plotted with the same isovalue, in which positive values of the wavefunctions are shown in red and negative in blue. According to this figure, the eigenstate wavefunction spread over nucleobase sites was observed for G, A, and C, but not for T. Similar to the local current, the eigenstate wavefunction decays as it is propagating to the sugar and phosphate group, and the wavefunction amplitude increases at the nanopore edge near the sugar-phosphate group. This analysis demonstrates that for each nucleotide the electron probability signatures lead to a local current modulation and are hence responsible for the distinction between each molecule.

Even though we were able to demonstrate a substantial potential of Mxene to successfully detect individual nucleotides for the purpose of DNA sequencing, certain limitations of the present study should be pointed out: First, we realize that the calculation approach which employs the gate electrode by tuning the Fermi energy employs a simplified approximation of determining the conductance. However, a very recent study on MXene-based FET has shown that the transmission as a function of gate voltage will not be significantly changed for a small bias [66]. Second, our study has been strictly limited to determining the conductance variation due to sampling over multiple positions and orientations without water molecules. Certainly, a more realistic simulation considering the presence of water would be most helpful for a deeper investigation of this nanopore-based DNA sequencing device. Recent theoretical studies [67] reported on the role of water on the electronic transport in graphene nanogap-based DNA sequencing devices, indicating an increase in conductance. In the case of Mxene nanopores, we assume that the water might not significantly affect the electrical properties due to its high intrinsic conductivity and low noise at room temperature. To verify our hypothesis, future studies should directly investigate the effect of fluctuating water environments on the electrical properties of Mxene nanopores.

4 Conclusions

In summary, the proposed $\text{Ti}_2\text{C}(\text{OH})_2$ MXene device allows for conductance measurements of the DNA translocation inside the nanopore with multiple orientations. Using a combination of DFT

and NEGF methods, we have shown that the device meets multiple performance requirements: It effectively distinguishes between the four naturally occurring nucleotides, and at the same time, it also helps to stabilize the DNA structures as they pass through the nanopore. By sweeping the gate voltage, the current pathway flowing through the device can be modulated in a way to enhance selectiveness toward the DNA nucleotides. In particular, when combined with MD simulations, the transverse conductance is clearly statistically distinguishable. Based on our results, one could extend future studies further to explore the use of MXenes with different pore sizes, variations in elemental compositions, alternative surface functionalization, conductance fluctuation due to the inclusion of an explicit water environment, and gate voltage adjustment to optimize the sensing capabilities for sequencing DNA. Understanding the influence of each factor on the electrical properties stemming from DNA translocation through the nanopore will provide guidance for the efficient design of a novel ultra-fast and accurate DNA sequencing device based on 2D MXene materials.

Acknowledgements

J. P. acknowledges support from the Thailand Research Fund (MRG6280150). S. J. is supported by Suranaree University of Technology (SUT), Thailand Science Research and Innovation (TSRI), and National Science, Research and Innovation Fund (NSRF grant No. B05F640051). R. G. A. thanks for financial support from CNPq (Nos. 437182/2018-5 and 313076/2020-0) and also FAPERJ (Nos. E-26/010.101126/2018 and 26/202.699/2019). R. H. S. acknowledges the Swedish Research Council (VR grant 2017-04627).

Funding note: Open access funding provided by Uppsala University.

Electronic Supplementary Material: Supplementary material (a more detailed discussion of MD trajectories of each nucleotide inside the $\text{Ti}_2\text{C}(\text{OH})_2$ nanopore and a linear response calculation of the conductance as function of the gate potential) is available in the online version of this article at <https://doi.org/10.1007/s12274-022-4632-8>.

Open Access This article is licensed under a Creative Commons Attribution 4.0 International License, which permits use, sharing, adaptation, distribution and reproduction in any medium or format, as long as you give appropriate credit to the original author(s) and the source, provide a link to the Creative Commons licence, and indicate if changes were made.

The images or other third party material in this article are

included in the article's Creative Commons licence, unless indicated otherwise in a credit line to the material. If material is not included in the article's Creative Commons licence and your intended use is not permitted by statutory regulation or exceeds the permitted use, you will need to obtain permission directly from the copyright holder.

To view a copy of this licence, visit <http://creativecommons.org/licenses/by/4.0/>.

References

- [1] Wheeler, D. A.; Srinivasan, M.; Egholm, M.; Shen, Y. F.; Chen, L.; McGuire, A.; He, W.; Chen, Y. J.; Makhijani, V.; Roth, G. T. et al. The complete genome of an individual by massively parallel DNA sequencing. *Nature* **2008**, *452*, 872–876.
- [2] Hayden, E. C. Technology: The \$1,000 genome. *Nature* **2014**, *507*, 294–295.
- [3] Mardis, E. R. The impact of next-generation sequencing technology on genetics. *Trends Genet.* **2008**, *24*, 133–141.
- [4] Ziegler, A.; Koch, A.; Krockenberger, K.; Großhennig, A. Personalized medicine using DNA biomarkers: A review. *Hum. Genet.* **2012**, *131*, 1627–1638.
- [5] Feng, Y. X.; Zhang, Y. C.; Ying, C. F.; Wang, D. Q.; Du, C. L. Nanopore-based fourth-generation DNA sequencing technology. *Genomics Proteomics Bioinformatics* **2015**, *13*, 4–16.
- [6] Venkatesan, B. M.; Bashir, R. Nanopore sensors for nucleic acid analysis. *Nat. Nanotechnol.* **2011**, *6*, 615–624.
- [7] Olasagasti, F.; Lieberman, K. R.; Benner, S.; Cherf, G. M.; Dahl, J. M.; Deamer, D. W.; Akeson, M. Replication of individual DNA molecules under electronic control using a protein nanopore. *Nat. Nanotechnol.* **2010**, *5*, 798–806.
- [8] Clarke, J.; Wu, H. C.; Jayasinghe, L.; Patel, A.; Reid, S.; Bayley, H. Continuous base identification for single-molecule nanopore DNA sequencing. *Nat. Nanotechnol.* **2009**, *4*, 265–270.
- [9] Stoloff, D. H.; Wanunu, M. Recent trends in nanopores for biotechnology. *Curr. Opin. Biotechnol.* **2013**, *24*, 699–704.
- [10] Dekker, C. Solid-state nanopores. *Nat. Nanotechnol.* **2007**, *2*, 209–215.
- [11] Foloea, D.; Uplinger, J.; Thomas, B.; McNabb, D. S.; Li, J. L. Slowing DNA translocation in a solid-state nanopore. *Nano Lett.* **2005**, *5*, 1734–1737.
- [12] Li, J. L.; Stein, D.; McMullan, C.; Branton, D.; Aziz, M. J.; Golovchenko, J. A. Ion-beam sculpting at nanometre length scales. *Nature* **2001**, *412*, 166–169.
- [13] Foloea, D.; Gershaw, M.; Ledden, B.; McNabb, D. S.; Golovchenko, J. A.; Li, J. L. Detecting single stranded DNA with a solid state nanopore. *Nano Lett.* **2005**, *5*, 1905–1909.
- [14] Gierhart, B. C.; Howitt, D. G.; Chen, S. J.; Zhu, Z. N.; Kotecki, D. E.; Smith, R. L.; Collins, S. D. Nanopore with transverse nanoelectrodes for electrical characterization and sequencing of DNA. *Sens. Actuators B: Chem.* **2008**, *132*, 593–600.
- [15] Tsutsui, M.; He, Y. H.; Furuhashi, M.; Rahong, S.; Taniguchi, M.; Kawai, T. Transverse electric field dragging of DNA in a nanochannel. *Sci. Rep.* **2012**, *2*, 394.
- [16] Fried, J. P.; Swett, J. L.; Nadappuram, B. P.; Mol, J. A.; Edel, J. B.; Ivanov, A. P.; Yates, J. R. In situ solid-state nanopore fabrication. *Chem. Soc. Rev.* **2021**, *50*, 4974–4992.
- [17] Wang, Z.; Lv, T. Y.; Shi, Z. B.; Yang, S. S.; Gu, Z. Y. Two-dimensional materials as solid-state nanopores for chemical sensing. *Dalton Trans.* **2021**, *50*, 13608–13619.
- [18] Choi, J.; Lee, C. C.; Park, S. Scalable fabrication of sub-10 nm polymer nanopores for DNA analysis. *Microsyst. Nanoeng.* **2019**, *5*, 12.
- [19] Yuan, Z. S.; Wang, C. Y.; Yi, X.; Ni, Z. H.; Chen, Y. F.; Li, T. Solid-state nanopore. *Nanoscale Res. Lett.* **2018**, *13*, 56.
- [20] Schneider, G. F.; Kowalczyk, S. W.; Calado, V. E.; Pandraud, G.; Zandbergen, H. W.; Vandersypen, L. M. K.; Dekker, C. DNA translocation through graphene nanopores. *Nano Lett.* **2010**, *10*, 3163–3167.
- [21] Merchant, C. A.; Healy, K.; Wanunu, M.; Ray, V.; Peterman, N.; Bartel, J.; Fischbein, M. D.; Venta, K.; Luo, Z. T.; Johnson, A. T. C. et al. DNA translocation through graphene nanopores. *Nano Lett.* **2010**, *10*, 2915–2921.
- [22] Garaj, S.; Hubbard, W.; Reina, A.; Kong, J.; Branton, D.; Golovchenko, J. A. Graphene as a subnanometre trans-electrode membrane. *Nature* **2010**, *467*, 190–193.
- [23] Van Den Hout, M.; Hall, A. R.; Wu, M. Y.; Zandbergen, H. W.; Dekker, C.; Dekker, N. H. Controlling nanopore size, shape and stability. *Nanotechnology* **2010**, *21*, 115304.
- [24] Yanagi, I.; Akahori, R.; Hatano, T.; Takeda, K. I. Fabricating nanopores with diameters of sub-1 nm to 3 nm using multilevel pulse-voltage injection. *Sci. Rep.* **2014**, *4*, 5000.
- [25] Balandin, A. A. Low-frequency 1/f noise in graphene devices. *Nat. Nanotechnol.* **2013**, *8*, 549–555.
- [26] Heerema, S. J.; Schneider, G. F.; Rozemuller, M.; Vicarelli, L.; Zandbergen, H. W.; Dekker, C. 1/f noise in graphene nanopores. *Nanotechnology* **2015**, *26*, 074001.
- [27] Waduge, P.; Larkin, J.; Upmanyu, M.; Kar, S.; Wanunu, M. Programmed synthesis of freestanding graphene nanomembrane arrays. *Small* **2015**, *11*, 597–603.
- [28] Rajan, A. C.; Rezapour, M. R.; Yun, J.; Cho, Y.; Cho, W. J.; Min, S. K.; Lee, G.; Kim, K. S. Two dimensional molecular electronics spectroscopy for molecular fingerprinting, DNA sequencing, and cancerous DNA recognition. *ACS Nano* **2014**, *8*, 1827–1833.
- [29] Liu, S.; Lu, B.; Zhao, Q.; Li, J.; Gao, T.; Chen, Y. B.; Zhang, Y. F.; Liu, Z. F.; Fan, Z. C.; Yang, F. H. et al. Boron nitride nanopores: Highly sensitive DNA single-molecule detectors. *Adv. Mater.* **2013**, *25*, 4549–4554.
- [30] Liu, K.; Lihter, M.; Sarathy, A.; Caneva, S.; Qiu, H.; Deiana, D.; Tileli, V.; Alexander, D. T. L.; Hofmann, S.; Dumcenco, D. et al. Geometrical effect in 2D nanopores. *Nano Lett.* **2017**, *17*, 4223–4230.
- [31] Liu, K.; Feng, J. D.; Kis, A.; Radenovic, A. Atomically thin molybdenum disulfide nanopores with high sensitivity for DNA translocation. *ACS Nano* **2014**, *8*, 2504–2511.
- [32] Waduge, P.; Bilgin, I.; Larkin, J.; Henley, R. Y.; Goodfellow, K.; Graham, A. C.; Bell, D. C.; Vamivakas, N.; Kar, S.; Wanunu, M. Direct and scalable deposition of atomically thin low-noise MoS₂ membranes on apertures. *ACS Nano* **2015**, *9*, 7352–7359.
- [33] Graf, M.; Lihter, M.; Altus, D.; Marion, S.; Radenovic, A. Transverse detection of DNA using a MoS₂ nanopore. *Nano Lett.* **2019**, *19*, 9075–9083.
- [34] Danda, G.; Das, P. M.; Chou, Y. C.; Mlack, J. T.; Parkin, W. M.; Naylor, C. H.; Fujisawa, K.; Zhang, T. Y.; Fulton, L. B.; Terrones, M. et al. Monolayer WS₂ nanopores for DNA translocation with light-adjustable sizes. *ACS Nano* **2017**, *11*, 1937–1945.
- [35] Naguib, M.; Kurtoglu, M.; Presser, V.; Lu, J.; Niu, J. J.; Heon, M.; Hultman, L.; Gogotsi, Y.; Barsoum, M. W. Two-dimensional nanocrystals produced by exfoliation of Ti₃AlC₂. *Adv. Mater.* **2011**, *23*, 4248–4253.
- [36] Naguib, M.; Mashtalir, O.; Carle, J.; Presser, V.; Lu, J.; Hultman, L.; Gogotsi, Y.; Barsoum, M. W. Two-dimensional transition metal carbides. *ACS Nano* **2012**, *6*, 1322–1331.
- [37] Anasori, B.; Lukatskaya, M. R.; Gogotsi, Y. 2D metal carbides and nitrides (MXenes) for energy storage. *Nat. Rev. Mater.* **2017**, *2*, 16098.
- [38] Mojtabavi, M.; VahidMohammadi, A.; Liang, W. T.; Beidaghi, M.; Wanunu, M. Single-molecule sensing using nanopores in two-dimensional transition metal carbide (MXene) membranes. *ACS Nano* **2019**, *13*, 3042–3053.
- [39] Yadav, P.; Cao, Z. L.; Farimani, A. B. DNA detection with single-layer Ti₃C₂ MXene nanopore. *ACS Nano* **2021**, *15*, 4861–4869.
- [40] Xue, Y. Q.; Datta, S.; Ratner, M. A. First-principles based matrix Green's function approach to molecular electronic devices: General formalism. *Chem. Phys.* **2002**, *281*, 151–170.
- [41] Brandbyge, M.; Mozos, J. L.; Ordejón, P.; Taylor, J.; Stokbro, K. Density-functional method for nonequilibrium electron transport. *Phys. Rev. B* **2002**, *65*, 165401.
- [42] Hohenberg, P.; Kohn, W. Inhomogeneous electron gas. *Phys. Rev.* **1964**, *136*, B864–B871.

- [43] Kohn, W.; Sham, L. J. Self-consistent equations including exchange and correlation effects. *Phys. Rev.* **1965**, *140*, A1133–A1138.
- [44] Perdew, J. P.; Burke, K.; Ernzerhof, M. Generalized gradient approximation made simple. *Phys. Rev. Lett.* **1996**, *77*, 3865–3868.
- [45] Smidstrup, S.; Markussen, T.; Vancraeyveld, P.; Wellendorff, J.; Schneider, J.; Gunst, T.; Verstichel, B.; Stradi, D.; Khomyakov, P. A.; Vej-Hansen, U. G. et al. QuantumATK: An integrated platform of electronic and atomic-scale modelling tools. *J. Phys.: Condens. Matter* **2019**, *32*, 015901.
- [46] Troullier, N.; Martins, J. L. Efficient pseudopotentials for plane-wave calculations. *Phys. Rev. B* **1991**, *43*, 1993–2006.
- [47] Zhang, Q. X.; Wei, J.; Liu, J. C.; Wang, Z. C.; Lei, M.; Quhe, R. 2D/2D electrical contacts in the monolayer WSe₂ transistors: A first-principles study. *ACS Appl. Nano Mater.* **2019**, *2*, 2796–2805.
- [48] Monkhorst, H. J.; Pack, J. D. Special points for Brillouin-zone integrations. *Phys. Rev. B* **1976**, *13*, 5188–5192.
- [49] Boys, S. F.; Bernardi, F. The calculation of small molecular interactions by the differences of separate total energies. Some procedures with reduced errors. *Mol. Phys.* **1970**, *19*, 553–566.
- [50] Fisher, R. S.; Lee, P. A. Relation between conductivity and transmission matrix. *Phys. Rev. B* **1981**, *23*, 6851–6854.
- [51] Solomon, G. C.; Herrmann, C.; Hansen, T.; Mujica, V.; Ratner, M. A. Exploring local currents in molecular junctions. *Nat. Chem.* **2010**, *2*, 223–228.
- [52] Paulsson, M.; Brandbyge, M. Transmission eigenchannels from nonequilibrium Green's functions. *Phys. Rev. B* **2007**, *76*, 115117.
- [53] Prasongkit, J.; Grigoriev, A.; Pathak, B.; Ahuja, R.; Scheicher, R. H. Transverse conductance of DNA nucleotides in a graphene nanogap from first principles. *Nano Lett.* **2011**, *11*, 1941–1945.
- [54] Prasongkit, J.; Feliciano, G. T.; Rocha, A. R.; He, Y. H.; Osotchan, T.; Ahuja, R.; Scheicher, R. H. Theoretical assessment of feasibility to sequence DNA through interlayer electronic tunneling transport at aligned nanopores in bilayer graphene. *Sci. Rep.* **2015**, *5*, 17560.
- [55] Prasongkit, J.; De Freitas Martins, E.; De Souza, F. A. L.; Scopel, W. L.; Amorim, R. G.; Amornkitbamrung, V.; Rocha, A. R.; Scheicher, R. H. Topological line defects around graphene nanopores for DNA sequencing. *J. Phys. Chem. C* **2018**, *122*, 7094–7099.
- [56] Sadeghi, H.; Bailey, S.; Lambert, C. J. Silicene-based DNA nucleobase sensing. *Appl. Phys. Lett.* **2014**, *104*, 103104.
- [57] Amorim, R. G.; Scheicher, R. H. Silicene as a new potential DNA sequencing device. *Nanotechnology* **2015**, *26*, 154002.
- [58] Kumawat, R. L.; Garg, P.; Kumar, S.; Pathak, B. Electronic transport through DNA nucleotides in atomically thin phosphorene electrodes for rapid DNA sequencing. *ACS Appl. Mater. Interfaces* **2019**, *11*, 219–225.
- [59] Fragasso, A.; Schmid, S.; Dekker, C. Comparing current noise in biological and solid-state nanopores. *ACS Nano* **2020**, *14*, 1338–1349.
- [60] Carson, S.; Wilson, J.; Aksimentiev, A.; Wanunu, M. Smooth DNA transport through a narrowed pore geometry. *Biophys. J.* **2014**, *107*, 2381–2393.
- [61] Li, J. L.; Talaga, D. S. The distribution of DNA translocation times in solid-state nanopores. *J. Phys.: Condens. Matter* **2010**, *22*, 454129.
- [62] Henry, M. B.; Tumbapo, M.; Tayo, B. O. Identification of DNA bases using nanopores created in finite-size nanoribbons from graphene, phosphorene, and silicene. *AIP Adv.* **2021**, *11*, 035324.
- [63] Chandiramouli, R.; Nagarajan, V. Silicene nanosheet device with nanopore to identify the nucleobases-a first-principles perspective. *Chem. Phys. Lett.* **2019**, *730*, 70–75.
- [64] Farimani, A. B.; Min, K.; Aluru, N. R. DNA base detection using a single-layer MoS₂. *ACS Nano* **2014**, *8*, 7914–7922.
- [65] Gouveia, J. D.; Morales-Garcia, A.; Viñes, F.; Illas, F.; Gomes, J. R. B. MXenes as promising catalysts for water dissociation. *Appl. Catal. B* **2020**, *260*, 118191.
- [66] Akkuş, Ü. Ö.; Balci, E.; Berber, S. Device characteristics of Ti₂CT₂ MXene-based field-effect transistor. *Superlattices Microstruct.* **2020**, *140*, 106433.
- [67] De Freitas Martins, E.; Amorim, R. G.; Feliciano, G. T.; Scheicher, R. H.; Rocha, A. R. The role of water on the electronic transport in graphene nanogap devices designed for DNA sequencing. *Carbon* **2020**, *158*, 314–319.